Transmembrane 163 (TMEM163) protein effluxes zinc

Vanessa B. Sanchez[1,§], Saima Ali[1], Adrian B. Escobar[1], and Math P. Cuajungco[1,2,*]

[1]Department of Biological Science, and [2]Center for Applied Biotechnology Studies, California State University Fullerton, CA, USA 92831

Running Title: *TMEM163 effluxes zinc*

***To whom correspondence should be addressed**:
Dr. Math P. Cuajungco
Department of Biological Science
California State University Fullerton
800 North State College Blvd, Fullerton, CA 92831
E-mail: mcuajungco@fullerton.edu
Tel: +1-657-278-8522
Fax: +1-657-278-3426

Keywords: SV31, zinc transporter, single nucleotide polymorphism, cation diffusion facilitator

ABSTRACT

Recent investigations of rodent Tmem163 suggest that it binds to and transports zinc as a dimer, and that alanine mutagenesis of its two species-conserved aspartate (D123A/D127A) residues perturbs its function. Direct corroboration, however, is lacking whether it is an influx or efflux transporter in cells. We hypothesized that human TMEM163 is a zinc effluxer based on its predicted protein characteristics. We used cultured human cell lines that either stably or transiently expressed TMEM163 and pre-loaded the cells with zinc to determine transport activity. We found that TMEM163-expressing cells exhibited significant reduction of intracellular zinc levels as evidenced by two zinc-specific fluorescent dyes and radionuclide zinc-65. The specificity of the fluorescence signal was confirmed upon treatment with TPEN, a high-affinity zinc chelator. Radionuclide zinc-65 assay revealed that the efflux activity of TMEM163 has an apparent Km value of 8 micro-molars. To further characterize the efflux function of TMEM163, we substituted alanine into two conserved aspartate residues (D124A/D128A) previously proposed as zinc binding sites. We also performed site-directed mutagenesis of several conserved amino acid residues identified as non-synonymous single nucleotide polymorphism (S61R, S95C, S193P, and E286K). We found a significant reduction of zinc efflux upon cellular expression of D124A/D128A or E286K protein variant when compared with wild-type, suggesting that these particular amino acids are important for normal protein function. Taken together, our findings demonstrate for the first time that TMEM163 effluxes zinc and is a new member of the cation diffusion facilitator (CDF) family that contributes to zinc homeostasis in specific cell types.

Abnormal extracellular zinc accumulation leading to cytosolic zinc overload has been shown to result in cytotoxicity *in vitro* and *in vivo*, which can be rescued by zinc-specific chelators (Choi *et al.*, 1988; Koh and Choi, 1994; Cuajungco and Lees, 1996; Koh *et al.*, 1996; Cuajungco and Lees, 1998; Kukic *et al.*, 2014). Many tissues and organs, therefore, have redundant

defense mechanisms to strictly maintain zinc homeostasis in order to prevent the cytotoxic effect of intracellular zinc elevation. Zinc homeostasis in mammalian cells is achieved by a tissue-specific and highly conserved low molecular weight zinc transport protein families called ZNT (SLC30, solute carrier 30A) and Zrt- and Irt-like protein (ZIP; SLC39) (Eide, 2006; Colvin *et al.*, 2010; Kambe *et al.*, 2014). The ZNT proteins are known to efflux zinc from the cytoplasm into the extracellular milieu and into the lumen of membrane-bound or vesicular compartments. The ZIP proteins, meanwhile, influx zinc from the outside of the cell into the cytoplasm and from the lumen of membrane-bound or vesicular compartments into the cytoplasm (Eide, 2006; Colvin *et al.*, 2010; Kambe *et al.*, 2014). In addition to ZNTs, the cells have secondary defense mechanisms to prevent cytoplasmic zinc overload and buffer intracellular zinc elevation, which is accomplished by metallo-proteins, amino acids such as histidine and cysteine, as well as small proteins such as metallothionein (MT) and glutathione (Itoh *et al.*, 1983; Aiken *et al.*, 1992; Horn *et al.*, 1995).

Zinc dyshomeostasis has been implicated in several human diseases such as schizophrenia (Scarr *et al.*, 2016), age-related macular degeneration (Smailhodzic *et al.*, 2014), Alzheimer's disease (Cuajungco and Lees, 1997a; b; Danscher *et al.*, 1997; Cuajungco *et al.*, 2000; Beyer *et al.*, 2009; Bosomworth *et al.*, 2013), Parkinson's disease-like dystonia (Aydemir *et al.*, 2017), amyotrophic lateral sclerosis (Kim *et al.*, 2009; Kaneko *et al.*, 2015), multiple sclerosis (Choi *et al.*, 2016), cerebral stroke (Koh *et al.*, 1996; Yoo *et al.*, 2004; Medvedeva *et al.*, 2009), and Mucolipidosis type IV (MLIV) (Cuajungco and Lees, 1997b; Eichelsdoerfer *et al.*, 2010; Cuajungco *et al.*, 2014; Smailhodzic *et al.*, 2014; Scarr *et al.*, 2016). In the case of MLIV, a neurodegenerative disease caused by the loss-of-function mutation in the transient receptor potential mucolipin-1 (TRPML1) ion channel, we found abnormal lysosomal zinc accumulation among zinc-treated MLIV patient fibroblasts and human embryonic kidney (HEK)-293 cells upon RNA interference (RNAi)-induced knock down of TRPML1 (Eichelsdoerfer *et al.*, 2010; Cuajungco *et al.*, 2014). We also observed increased tissue zinc levels in post-mortem brain of Trpml1-null mice (Eichelsdoerfer *et al.*, 2010). Our interest in human TMEM163 stemmed from these observations and our recent finding that TMEM163 interacts with TRPML1 (Cuajungco *et al.*, 2014). Rodent Tmem163, also known as synaptic vesicle 31 (SV31), was first identified from rat brain synaptosomes using proteomics analysis and was shown to bind zinc, nickel, and copper (Burre *et al.*, 2007). Tmem163 has been detected in certain types of glutamatergic and γ-aminobutyric acid (GABA)-ergic neuronal populations (Burre *et al.*, 2007; Barth *et al.*, 2011). Barth *et al.* (2007) used immunocytochemistry and subcellular fractionation studies of neuron-like PC-12 cells stably expressing rodent Tmem163 to reveal that this protein is detected mostly in the plasma membrane (PM), lysosomes, early endosomes, and other vesicular compartments especially synaptic vesicles (Barth *et al.*, 2011). Confocal microscopy studies of heterologously expressed TMEM163 in HEK-293 cells revealed that it localizes in the PM and lysosomes as well (Cuajungco *et al.*, 2014). Our analysis shows that TMEM163 transcripts are detected in many tissues, notably in the brain, lung, pancreas, kidney, ovary, and testis (Cuajungco *et al.*, 2014); however, mouse Tmem163 was reported to be exclusively expressed in the brain (Burre *et al.*, 2007).

Previously, it was shown that purified rodent Tmem163 protein reconstituted in liposomes forms a dimer and transports zinc in a proton-dependent manner (Waberer *et al.*, 2017). It was also shown that Tmem163's ability to bind and transport zinc becomes inactivated upon alanine substitution of two species-conserved aspartate residues at position 123 and 127 (i.e. Tmem163-D123A/D127A). Thus, the data indicate that these double aspartate residues are zinc binding sites, but that they do not affect Tmem163 dimerization (Waberer *et al.*, 2017). Note, however, that this particular study did not address the question of whether the protein serves to transport zinc in or out of living cells. In the current report, we reveal for the first time that human TMEM163 is a zinc efflux transporter using radionuclide zinc-65 and zinc-specific fluorescent dyes. Amino acid substitution of species-conserved amino acid residues shown to disrupt zinc binding and potentially alter protein conformation negatively affects the zinc efflux function of TMEM163. Overall, these observations indicate that TMEM163 should be designated as a new member of the cation diffusion facilitator (CDF) family of zinc efflux transporters that are crucial to maintaining zinc homeostasis in living organisms.

EXPERIMENTAL PROCEDURES

Bioinformatics analysis

We performed bioinformatics analysis (www.expasy.org) of TMEM163 using TMPred (Hofmann and Stoffel, 1993) and TMRPres2d (Spyropoulos *et al.*, 2004) to determine and visualize its predicted transmembrane domain and topology. To identify amino acid residues subject to post-translational modification (PTM) within TMEM163, we

searched the UniProt database (https://www.uniprot.org/uniprot/Q8TC26) and found several PTM entries from the PhosphoSitePlus® (https://www.phosphosite.org/proteinAction?id=24760) website as potential phosphorylation sites. We also performed a Clustal W sequence alignment using Lasergene MegAlign v. 15 (DNAStar, Madison, WI) to show amino acid sequence conservation among several vertebrate species. To show amino acid sequence similarity of specific protein regions or domains between TMEM163 and select CDF family of zinc transporters, we used the Multiple Alignment using Fourier Transform (MAFFT) online resource, which also allowed us to determine the phylogenetic relationship among the proteins (https://mafft.cbrc.jp/alignment/server/).

To address the previous report that mouse Tmem163 is exclusively expressed in the brain, we obtained the existing Mouse ENCODE transcriptome data (Accession no. PRJNA66167) from the National Center for Biotechnology Information (NCBI) website (https://www.ncbi.nlm.nih.gov/gene/?term=Mus+musculus+Tmem163#gene-expression). We re-arranged the tissue positions to highlight the presence of Tmem163 transcripts present in other tissues.

We used the single nucleotide polymorphism (SNP) database from NCBI (dbSNP; www.ncbi.nlm.nih.gov/snp) to identify specific nucleotide sequence variations within the *TMEM163* gene that result in non-synonymous amino acid substitutions. (**Supplemental Table S1**). Based on the predicted secondary structure information we obtained from several online resources (e.g. NCBI, UniProt), we selected four non-synonymous SNPs that we surmised to disrupt TMEM163's native structure and function, namely: Serine to Arginine at position 61 (S61R), Serine to Cysteine at position 95 (S95C), Serine to Proline (S193P), and Glutamate to Lysine at position 286 (E286K). These SNPs were PCR-cloned using the primer sets outlined in **Supplemental Table S2**. Note that the PhosphoSitePlus website mentioned above shows that Serine at position 61 is a phosphorylation site (**Supplemental Table S3**).

Cell culture

Human embryonic kidney (HEK)-293 and HeLa cells were purchased from American Type Culture Collection (ATCC; Manassas, VA). We cultured HeLa and HEK-293 cells in Dulbecco's Modified Eagle's Media (DMEM; 4.50 g/L glucose, 0.58 g/L L-glutamine, 0.11 g/L sodium pyruvate; Corning) supplemented with 10% fetal bovine serum (FBS; Thermo Scientific, Waltham, MA), but without antibiotics. The cells were maintained in a humidified 37°C incubator supplied with 5% CO_2.

Creation of stable cell lines

We created HeLa cells that stably over-express an empty pmCherry vector control (Takara Bio, Mountain View, CA), a monomeric red fluorescent protein variant (ex = 587 nm, em = 610 nm) (Shaner *et al.*, 2004) and a TMEM163 construct with mCherry fused at the C-terminus region (Cuajungco *et al.*, 2014). Endogenous *TMEM163* transcripts are not detected in HeLa cells (www.proteinatlas.org). The pmCherry N1 vector contains a *Neomycin* resistance gene driven by the SV40 promoter. The TMEM163-mCherry and empty pmCherry vectors were linearized using the *Not I* restriction site and column-purified. The linearized vectors were transfected with TurboFect into a 70% confluent HeLa cells cultured in a 6-well plate. Every two to three days, the DMEM media containing the G418 antibiotic (0.9 mg/mL) was replaced. After two weeks, most of the untransfected cells were dead and the islands of transfected cells exhibiting red fluorescence viewed under an inverted IX-71 Olympus fluorescent microscope (Olympus America, Center Valley, PA) were isolated using cloning cylinders held in place by 1% agarose. The cloning cylinders acted as small wells from which the clonal group could be trypsinized. The dissociated colony cells were re-seeded into a 24-well culture plate. The process was repeated several times to guarantee that untransfected cells were eliminated. We then used fluorescence microscopy to corroborate that each cell line was stably expressing TMEM163 or the plasmid. As additional verification, total RNA was extracted from the stable cell lines using Trizol (Thermo Scientific), and the purified RNA samples were reverse-transcribed to generate cDNAs. The veracity of stable gene expression was established by a standard polymerase chain reaction technique using specific primer sets that anneal only to the mCherry cDNA sequence or the mCherry-tagged *TMEM163* cDNA sequence.

RNA interference (RNAi)

We used a short hairpin RNA (shRNA, 29-mer; OriGene Technologies, Rockville, MD) expression vector that effectively down-regulates TMEM163 expression. Expression validation of shRNA knockdown using PCR and Western blot can be found in the last supplemental figure of our previous report ((Eichelsdoerfer *et al.*, 2010; Cuajungco *et al.*, 2014). For this study, we seeded 15,000 HEK-293 cells per well in PDL-treated 96-well culture plate the day before the experiments. Cells in quadruplicate wells were

transfected with 2 µg DNA of either TMEM163-KD (knock-down) shRNA or TMEM163-OE (over-expression) construct using TurboFect lipid reagent (Thermo Scientific). Twenty-four hours post-transfection, the cells were washed three times with phosphate-buffered saline (PBS), exposed to low levels of exogenous zinc chloride ($ZnCl_2$, 100 nM) overnight, and washed three times with PBS before the spectrofluorometric assay.

Recombinant DNA constructs and site-directed mutagenesis (SDM) technique

We used a TMEM163-mCherry expression construct (Eichelsdoerfer *et al.*, 2010; Cuajungco *et al.*, 2014) to change a specific amino acid sequence corresponding to the non-synonymous TMEM163 SNPs used in the study (**Supplemental Table S2**). Using the online In-Fusion™ HD (IF) cloning system primer design website (Takara Bio USA, Mountain View, CA), we made primer sets for TMEM163 SNP, ZIP1 (a kind gift of Dr. David J. Eide, University of Wisconsin), and the TMEM163 double aspartate to alanine substitution mutation located at positions 124 and 128 (D124A/D128A) (**Supplemental Table S3**). Note that the double aspartate to alanine mutations were recently reported to decrease zinc binding and inactivate protein function in rodent Tmem163 at positions 123 and 127 (Tmem163-D123A/D127A) (Waberer *et al.*, 2017). Following SDM, we verified the DNA sequence integrity of all expression constructs by commercial sequencing (Retrogen, San Diego, CA) and analyzed the clone sequences using Lasergene SeqMan v. 15 (DNAStar, Madison, WI).

Spectrofluorometric assays using Fluozin-3 and Newport Green fluorescent dyes

RNAi expression

Following RNAi and exposure to zinc, the cells were washed three times with PBS. The cells were incubated with 1 µM of cell membrane permeable Fluozin-3 acetoxy-methyl ester (AM) fluorescent dye (MP-FZ3; Kd = 15 nM; ex = 494 nm, em = 516 nm; Thermo Scientific). Fluozin-3 is a well-established tool for evaluating changes in relative zinc levels due to its specificity, high dissociation constant, and physiological stability (Zhao *et al.*, 2008). The dye only emits fluorescence when bound to labile or chelatable zinc and the dye remains in the cytoplasm upon ester cleavage of the AM moiety (Gee *et al.*, 2002). We followed the manufacturer's recommendation to incubate MP-FZ3 for 30 minutes inside a 37°C incubator injected with 5% CO_2. The cells were then washed with PBS three times before performing an end-point assay for intracellular zinc fluorescence as previously described (Eichelsdoerfer *et al.*, 2010; Cuajungco *et al.*, 2014). Untransfected negative control cells were included in all experiments (n = 4 independent trials). Background fluorescence was subtracted (blank) from each treatment group to obtain the relative fluorescence unit (RFU). The data were analyzed using Prism 8.2 software (GraphPad, San Diego, CA).

Stable cell expression

We optimized the assay for cell membrane impermeable Fluozin-3 (MI-FZ3) and membrane permeable Newport Green dichloro-fluorescein-AM (MP-NG; Kd ~ 1 µM; ex = 505 nm, em = 535 nm; Thermo Scientific) spectrofluorometric assays by identifying the appropriate: (i) cell density; (ii) concentration of exogenous $ZnCl_2$; (iii) concentration of MI-FZ3 or MP-NG; and (iv) buffer types for dye incubation and washing. We also supplemented the incubation and wash buffers with 2 mM Glutamax™ (Thermo Scientific) and 1 mM sodium pyruvate to maintain cell viability throughout the period of experimentation.

We used HeLa cells stably expressing TMEM163-mCherry or pmCherry empty vector control. We seeded 25,000 cells per well in a PDL-treated 96-well plate one day before the experiments. The first six wells of each row were designated as treatment group (zinc exposed), while the remaining six wells in the same row were used as untreated control group (non-exposed). We then exposed the cells to $ZnCl_2$ (10 µM) and zinc pyrithione (1 µM) for 5 minutes and washed three times with HEPES buffer (15 mM HEPES, 100 mM D-glucose, and 150 mM KCl; pH 7.0) using an automated BioTek 405 TS microplate washer (BioTek Instruments, Winooski, VT). A post-washed volume of 100 µL was dispensed and the plate was transferred into the BioTek Cytation V plate reader and each well was dispensed with 100 µL HEPES buffer containing MI-FZ3 dye to a final concentration of 1 µM. We performed kinetic readings for each well every minute for 25 minutes. Average background RFU from non-zinc exposed group (transfected and non-transfected, but not pre-loaded with zinc) was subtracted from RFUs of zinc-exposed group (transfected and non-transfected). Background subtraction minimizes or prevents the confounding effects contributed by native zinc transporters present in cells such as ZNTs and ZIPs, which are both expressed in HeLa and HEK-293 cell lines (Human Protein Atlas, www.proteinatlas.org). Five-minute data point intervals were collected and analyzed using Prism 8.2 software.

To further support the MI-FZ3 results, we then performed assays using MP-NG. HeLa cells stably expressing TMEM163 and pmCherry vector control were seeded at 25,000 cells per well in a PDL-treated 96-well plate. The cells were incubated with MP-NG (5 μM) for 20 minutes inside a 37°C incubator injected with 5% CO_2, washed two times with a standard buffer (10 mM HEPES, 135 mM NaCl, 5 mM KCl, 1 mM $CaCl_2$, 1 mM $MgSO_4$, and 5 mM glucose; pH 7.4), and left at room temperature for another 30 minutes to ensure complete ester cleavage of AM moiety. The treatment group was exposed to $ZnCl_2$ (100 μM) and pyrithione (10 μM) for 20 minutes inside the incubator, washed five times with standard buffer, and each well was dispensed with a final volume of 100 μL standard buffer after the last wash. A kinetic reading for zinc flux was performed every minute for 45 minutes using the BioTek Cytation V plate reader. Background extracellular MI-FZ3 RFU levels (no zinc exposure) were subtracted from the zinc-treated RFU levels. We adapted a previously described protocol (Ohana *et al.*, 2009) to quantify changes in cytoplasmic zinc levels by dividing the RFU timepoint readings with the baseline RFU taken at time zero. Data points from 5-minute interval reads were collected and analyzed using Prism 8.2 software.

Transient cell expression

To further corroborate the stable expression data and include additional controls, we performed transient transfection of the following constructs: pmCherry empty vector, TMEM163-mCherry, ZIP1-mCherry (a known influx transporter), and TMEM163-D124/D128A-mCherry (a similar double mutation reported to inactivate rodent Tmem163) (Waberer *et al.*, 2017). We seeded HEK-293 cells at 15,000 cells per well on a 96-well culture plate treated with PDL one day before transfection. The first six wells of each row were designated as treatment group (zinc exposed), while the remaining six wells in the same row were used as untreated control group (non-exposed). We transfected the cells with 150 ng of DNA constructs per well using TurboFect lipid reagent. A standard amount of 200 ng DNA was then used per well for the empty vector control to match the efficiency of transfection in cells treated with the expression constructs containing a specific gene. Twenty-four hours post-transfection, the culture medium was aspirated, and each well was dispensed 100 μL of HEPES buffer with zinc (treated) or without zinc (untreated). The treated cells were exposed to $ZnCl_2$ (10 μM) and zinc pyrithione (1 μM) for 5 minutes in a humidified 37°C incubator supplied with 5% CO_2. The cells were then washed three times with HEPES buffer using an automated BioTek 405 TS microplate washer to minimize or prevent cells from lifting out of the well surface, and after the final liquid aspiration, each well was dispensed with 100 μL of HEPES buffer containing MI-FZ3 dye to a final concentration of 1 μM. The plate was transferred into the BioTek Cytation V plate reader and each well was assayed (kinetic reading) for zinc flux every minute for 25 minutes. To analyze the raw data, the background RFU values (no zinc exposure) were subtracted from zinc-treated RFU data as described earlier. Five-minute data point intervals were collected and analyzed using Prism 8.2 software.

To show that the MI-FZ3 fluorescence signal is directly attributable to zinc, we used the metal chelator N,N,N,N-*tetrakis*-(2-pyridylmethyl)-ethylenediamine (TPEN, 10 μM) in several transient transfection experiments as described earlier by injecting the chelator half-way through the kinetic reading. TPEN is a zinc-specific, high affinity chelator (Kd = 10^{-16} M) that binds chelatable zinc *in vivo* (Cuajungco and Lees, 1996; 1998) or *in vitro* (Zalewski *et al.*, 1993; Ahn *et al.*, 1998). One-minute interval reads were graphed using Prism 8.2 software.

To evaluate the effects of each non-synonymous SNP on TMEM163 function, we seeded HEK-293 at 15,000 cells per well in a PDL-treated 96-well plate the day before the experiment. Similar to the above approach for MI-FZ3, the first six wells were designated as zinc-treated group, while the last six wells were used as non-zinc treated group. We used TurboFect to transfect the cells with the following non-synonymous SNP-associated constructs (150 ng DNA): TMEM163-S61R-mCherry, TMEM163-S95C-mCherry, TMEM163-S193P-mCherry, and TMEM163-E286K-mCherry. Twenty-four hours post transfection, the cells were pre-loaded with $ZnCl_2$ (10 μM) and zinc pyrithione (1 μM) for 20 minutes, washed twice with HEPES buffer, and transferred to the plate reader for kinetic reading after injection of the MI-FZ3 dye (1 μM). A kinetic reading for zinc flux was performed every minute for 25 minutes using the BioTek Cytation V plate reader and the background RFU values were subtracted from the zinc-treated RFU values. Data points every 5 minutes were collected for analysis using Prism 8.2 software.

Radionuclide zinc-65 uptake assay

We purchased radionuclide zinc-65 (^{65}Zn, 1 μCi; Perkin Elmer, Waltham, MA) and followed published zinc flux assay protocol by the Eide laboratory with minor modifications to suit our experiments. HeLa cells stably expressing TMEM163-mCherry or pmCherry vector were seeded at 200,000 cells per well in a 12-

well culture plate treated with PDL. The cells were allowed to settle inside the cell culture incubator for 24 hours prior to treatment. Each treatment was done in duplicate wells, and a parallel plate for normalization using total protein levels was included in each experiment. We used an uptake buffer (15 mM HEPES, 100 mM glucose and 150 mM KCl; pH 7.0) to expose the cells with "hot" zinc (i.e. ^{65}Zn mixed with a "cold" $ZnCl_2$ solution). The hot zinc treatment solution was serially diluted with uptake buffer by half to obtain the following concentrations: 40, 20, 10, 5. 2.5 and 1.25 µM. We placed the ^{65}Zn-treated cells for 15 minutes inside a 37°C incubator injected with 5% CO_2, took them out, and then put them on ice. We added 250 µl of a stop buffer solution (1 mM EDTA added to uptake buffer) to chelate extracellular zinc in the milieu. EDTA is a membrane impermeable chelator that binds zinc (Kd = 10^{-16} M) (Cuajungco and Lees, 1998; Frederickson *et al.*, 2002). We used the standard buffer (10 mM HEPES, 135 mM NaCl, 5 mM KCl, 1 mM $CaCl_2$, 1 mM $MgSO_4$, and 5 mM glucose; pH 7.4) to wash the cells three times post-EDTA chelation. After the last wash, the buffer was aspirated and replaced with a standard lysis buffer (50 mM Tris-HCl, 150 mM NaCl, 1% Nonidet P-40, 1 mM EDTA, 0.25% sodium deoxycholate, 0.1% SDS and 1X protease inhibitor cocktail (Sigma-Aldrich, St. Louis, MO). The untreated plate was also lysed for subsequent use in total protein assay. The ^{65}Zn-treated cell lysates were assayed for radioactivity in counts per minute (cpm) using a scintillation counter. Using the information provided by the manufacturer regarding the specific activity of ^{65}Zn, we converted the cpm data to pmol per minute. The relative total protein concentration of lysates from TMEM163-mCherry and pmCherry-expressing cells were quantified (in milligrams) using the Pierce Bicinchoninic acid (BCA) assay kit according to the manufacturer's protocol (Thermo Fisher Scientific). The intracellular ^{65}Zn levels were then normalized by the total protein values. The Michaelis Menten (Km) value was calculated using the Lineweaver-Burk equation, and we also used the non-linear curve fit (Michaelis Menten) analysis in Prism 8.2 software to verify the Km and Vmax values of zinc efflux transport activity. We used Prism 8.2 to determine statistical significance between TMEM163 and control samples (n = 3 independent trials).

Immunocytochemistry (ICC) and fluorescence microscopy analysis

HEK-293 cells were seeded in sterile coverslips at approximately 30% confluency one day before transfection of the following expression constructs: TMEM163 wild-type (TMEM163-WT), TMEM163-D124A/D128A, TMEM163-S61R, TMEM163-S95C, TMEM163-S193P, TMEM163-E286K, ZIP1, and pmCherry vector control. The mammalian expression constructs used in the study either contained a fluorescent (mCherry; Takara Bio) protein tag or peptide tag (Myc-DDK; OriGene Technologies).

For mCherry-tagged constructs, we checked for transfection efficiency and the health of treated cells at 24 hours post-transfection before processing the cells for microscopy. The cells were fixed with 4% paraformaldehyde for 15 minutes, and washed three times with 1X PBS. Fluorescence imaging was done using an inverted Olympus IX-71 fluorescence microscope. Monochromatic RGB images of cells were captured using the CellSens software version 1.18 (Olympus). We then used Adobe Photoshop CC 2017 (Adobe Systems, San Jose, CA) to show the images in red color as represented by the mCherry fluorescence.

For Myc-DDK-tagged constructs, the cells were fixed with 4% paraformaldehyde for 15 minutes, washed three times with PBT1 buffer (1X PBS, 1% Triton-X 100, 0.1% BSA, 5% heat-inactivated goat serum) and incubated with primary antibody (1:1000 anti-DDK monoclonal 4C5; OriGene Technologies) in PBT1 at 4°C overnight. The cells were washed with PBT2 buffer (1X PBS, 1% Triton-X 100, 0.1% BSA) three times, and then incubated with secondary antibody (1:500 anti-mouse Alexa Fluor-488; ex = 490 nm, em = 525 nm; Thermo Scientific) in PBT2 for 2 hours at 4°C. The cells were then washed two times with 1X PBS. Each coverslip was mounted on a slide, treated with Prolong Gold anti-fade reagent and the edge of the coverslip was sealed with clear nail polish. Monochrome images were taken using an upright Olympus BX51 fluorescence microscope and processed using Adobe Photoshop CC 2017 to change the monochrome images to green color as represented by Alexa-488 fluorescence.

Cell viability assay

To investigate whether the SNPs and the TMEM163-D124A/D128A constructs affect cell health, we seeded 15,000 HEK-293 cells in a PDL-treated 96-well plate. Cells in quadruplicate wells were transfected with TMEM163-WT, TMEM163-D124A/D128A, TMEM163-S61R, TMEM163-S95C, TMEM163-S193P, TMEM163-E286K, and pmCherry empty vector control. We then assessed cell viability of treated and control cells 48 hours post-transfection using the CellTiter Glo 2.0 luciferase assay kit (Promega, Madison, WI) according to the manufacturer's protocol. The data were normalized

using un-transfected control cells and represented as percentage of control, and statistical significance was analyzed using Prism 8.2 software (n = 5 independent trials).

Cell surface biotinylation (CSB) and Western blot (WB)

HeLa cells were seeded at 1.5 x 10^6 cells in a 10-cm petri dish coated with PDL. We transfected the cells with Myc-DDK peptide tag plasmids (4 µg) using TurboFect lipid reagent as follows: TMEM163-WT, TMEM163-S61R, TMEM163-S95C, TMEM163-S193P, TMEM163-E286K and TMEM163-D124A/D128A. Twenty four hours post-transfection, the cells were washed two times with 10 ml of ice-cold PBS-CM (1X PBS, 0.5 mM $CaCl_2$, 1 mM $MgCl_2$; pH 8.0) and incubated with 1 ml of freshly prepared Sulfo-NHS-LC-LC-Biotin solution (Thermo Scientific; 0.5 mg/ml in PBS-CM) for 30 min at 4°C. The cells were washed twice with 10 ml of PBS-CM containing 0.1% BSA to terminate and quench any unbound Sulfo-NHS-LC-LC-Biotin. The cells were lysed for 1 hour at 4°C with 1 ml of lysis buffer (1X protease inhibitor cocktail, 1mM PMSF, 150 mM NaCl, 5 mM EDTA, 1% Nonidet P-40, 50 mM Tris; pH 7.5). The lysates were centrifuged at 14,000 rpm for 15 min at 4°C. An aliquot (1-5%) was taken from each sample to normalize total protein (input) levels for each treatment. The neutravidin beads (150 µl; Thermo Scientific) were equilibrated in lysis buffer, added to each protein sample (normalized to 680 µg total protein), and incubated overnight at 4°C. The samples were washed five times with lysis buffer, incubated in 60 µl Laemmli sample buffer for 30 min at 37°C, and eluted by low speed centrifugation. The samples were immunoblotted with primary anti-DDK monoclonal mouse antibody (Origene Technologies), and secondary anti-mouse IR-Dye 800CW (LI-COR Biosciences). The blots were then scanned using the Odyssey SA™ infrared imaging system (LI-COR Biosciences).

Statistical analysis

All numerical data were graphed and analyzed for statistical significance using Prism 8.2 software (GraphPad, La Jolla, CA). We used Student's *t*-test (two-tailed) to determine statistical significance of data from various zinc flux assays using stable cells expressing TMEM163 and pmCherry vector control. The Km and Vmax values of efflux transport activity were obtained using the non-linear curve fit analysis on Prism. Data obtained from other spectrofluorometric experiments were analyzed using one-way analysis of variance (ANOVA) with repeated measures and Tukey's multiple comparisons *post-hoc* test. The significance level was set at $p < 0.05$. Unless specified, all data evaluated for statistical significance are represented as mean ± SEM with at least three independent trials.

RESULTS

TMEM163 is a zinc effluxer

TMEM163 has six predicted transmembrane (TM) domains and is highly conserved among the vertebrate species we analyzed (**Supplemental Figure S1**). RNAi of TMEM163 in HEK-293 cells produced a substantial increase of intracellular MP-FZ3 fluorescence, while over-expression of TMEM163 displayed an opposite effect (**Supplemental Figure S2**). This result confirmed and was consistent with our previous report (Cuajungco *et al.*, 2014). Thus, we had an *a priori* information that TMEM163 may be transporting zinc out of living cells, but needed more evidence to substantiate this observation.

For this study, we used two different types of human cell lines, two heterologous expression systems (i.e. stable and transient), and three zinc flux assays to show the specificity and reproducibility of our observations that TMEM163 is an efflux transporter. To first show that TMEM163 effluxes zinc, we used HeLa cells stably expressing TMEM163 and analyzed zinc flux upon exogenous zinc exposure using two zinc-specific fluorescence dyes, MI-FZ3 or MP-NG. For MI-FZ3 assay, we found a substantial increase in extracellular fluorescence among TMEM163-expressing cells in comparison to the pmCherry control (**Fig.1A**). For MP-NG, a substantial reduction of intracellular MP-NG fluorescence was observed from cells expressing TMEM163 when compared to the pmCherry control (**Fig. 1B**). To provide additional evidence confirming our fluorescence data that TMEM163 is a zinc efflux transporter, we exposed HeLa cells stably expressing TMEM163-mCherry and mCherry with radionuclide ^{65}Zn. We found that TMEM163-expressing cells significantly reduced intracellular ^{65}Zn when compared with control cells (**Fig.1C**). The exogenous zinc uptake was concentration-dependent and saturable, with an apparent Michaelis-Menten fit (Km) for TMEM163's transport activity being equal to 8 ± 1 µM and a maximal velocity (Vmax) of 98 ± 5 pmol/min/mg total protein. We investigated that possibility that TMEM163 is indeed a member of the CDF family of zinc efflux transporters by performing a multiple sequence alignment and phylogenetic tree analyses of its amino acid residues and non-mammalian CDF proteins YiiP, CzcD, and ZitB, as well as mammalian CDF proteins ZNT1 through ZNT10 (**Supplemental Figure S3**). We

confirmed that TMEM163 shared conserved zinc-binding sites consisting of two aspartic acid residues within TM2. In addition, we identified aspartic residues located within TM5 and TM6 that are also potential zinc-binding regions, which are conserved or shared by distinct CDF members. Lastly, the phylogenetic relationship among CDF proteins demonstrated that TMEM163 is more related to ZNT9 in comparison to other CDF family members analyzed.

Loss-of-function mutation negatively affects TMEM163 function but not membrane localization

We looked at the effects of transient heterologous expression of TMEM163 in HEK-293 cells. In addition to pmCherry empty vector control, we used ZIP1 (a zinc influx transporter), and the double aspartate to alanine substitutions, TMEM163-D124A/128A. These alanine mutations are equivalent to rodent Tmem163-D123A/D127A that was previously reported as an inactive protein (Waberer *et al.*, 2017). We observed a discernable increase of MI-FZ3 fluorescence in the extracellular milieu of TMEM163-expressing cells, but not among cells expressing pmCherry empty vector control, ZIP1, and TMEM163-D124A/D128A (**Fig. 2A**). Statistical analysis using ANOVA with repeated measures, and *post-hoc* analysis using Dunnett's multiple comparisons test showed significant differences between TMEM163 and: i) TMEM163-D124A/D128A ($p < 0.0001$); ii) ZIP1 ($p < 0.0001$); and iii) pmCherry ($p = 0.002$). To demonstrate that the MI-FZ3 fluorescence signal is contributed by zinc extrusion in the extracellular environment, we performed additional experiments in which we injected TPEN during the kinetic measurement. TPEN is a high affinity, cell membrane permeant chelator that binds tightly to zinc (Cuajungco and Lees, 1996; 1998). We found that TPEN completely abrogated the MI-FZ3 fluorescence signal (**Supplemental Fig. S4**).

We wanted to ensure that the marked difference in zinc efflux activity between TMEM163-WT and TMEM163-D124A/D128A was not caused by either transfection or cell expression issues. We therefore took fluorescent images of the cells for evidence of transfection before performing the assays. We also performed fluorescence microscopy to determine the expression profiles of all four constructs. Our findings revealed that TMEM163 is localized within the plasma membrane (PM) and intracellular membrane compartments (MC) (**Fig. 2B**), which further confirmed our previous report (Cuajungco *et al.*, 2014). Interestingly, the subcellular localization of TMEM163-D124A/D128A appeared to be similar to the wild-type protein where it is detected in both the PM and MC. ZIP1 expression was detected in the PM and more prominently within MC, which happened to be consistent with previous reports (Gaither and Eide, 2001; Wang *et al.*, 2004a). As expected, the pmCherry empty vector was mainly observed in the cytoplasm.

Missense mutations in conserved amino acid residues negatively affects the zinc efflux function of TMEM163

Based on the apparent lack of transport activity by the D124A/D128A variant, we hypothesized that a single point mutation within certain conserved amino acid residues could potentially disrupt, if not also abolish, the normal efflux function of TMEM163. To avoid simply selecting amino acids based on information from prediction software tools, we strategically looked at specific non-synonymous SNPs that have been identified within the *TMEM163* gene using NCBI's dbSNP database (**Supplemental Table S1**). We picked four non-synonymous SNPs of serine (i.e. S61R, S95C, and S193P) and glutamic acid (i.e. E286K) residues due to their species conservation, position within the predicted secondary structure, and possible target for post-translational modification (**Supplemental Figure S5**). While amino acid substitution within serine (phosphorylation target) or glutamic acid (negatively charged) residue may negatively impact protein structure and function, our online analysis suggested that only S61 is a PTM site (**Supplemental Table S3**). We transiently expressed the non-synonymous SNP constructs in HEK-293 cells along with wild-type TMEM163 and pmCherry empty vector control. For this set of experiments, we incubated the cells with zinc and pyrithione for an extra 15 minutes than the previous experiments on transient TMEM163 expression in cells, in order to gauge whether the amino acid substitution could also affect cell health after a longer zinc exposure. We found that the cells expressing the SNP constructs showed significant reductions in extracellular MI-FZ3 fluorescence signal when compared with wild-type TMEM163 (**Fig. 3A**). ANOVA with repeated measures and *post-hoc* analysis using Dunnett's multiple comparisons test showed significant differences between wild-type TMEM163 and: i) S61R ($p = 0.001$); ii) S95C ($p = 0.04$); S193P ($p = 0.0004$); and iii) E286K ($p = 0.0005$). The MI-FZ3 fluorescence signals coming from cells expressing S61R, S95C, and S193P constructs were very similar to that of cells expressing the pmCherry empty vector control. Note, however, that the cells expressing the E286K construct displayed the lowest efflux activity, which was well below the fluorescence obtained from pmCherry empty vector control (**Fig. 3A**) and slightly resembled the efflux activity of D124A/D128A protein variant.

Most of the TMEM163 variant alleles localize to the plasma membrane and do not affect cell viability

Similar to our earlier experimental approach, we captured fluorescence images of the cells expressing the SNPs to determine transfection efficiency and expression profile before we performed each MI-FZ3 assay. Fluorescence microscopy analyses of SNP constructs tagged with mCherry fluorescent protein or Myc-DDK peptide showed a very similar expression pattern to the wild-type TMEM163 protein despite differences in their efflux activity (**Fig. 3B**). It is worth noting that the S193P expression profile with mCherry tag appeared exclusively within the cytoplasm, which was very similar to cells expressing the empty pmCherry vector control. On the other hand, S193P with Myc-DDK tag was mainly localized within MC but was also detected in PM. Cell surface protein analysis using CSB and WB showed that all SNPs, including the D124A/D128A were detected within the PM; however the level of S193P protein variant was markedly reduced in the PM relative to the normalized samples of other SNPs (elute) (**Fig. 4**). The CSB and WB data also revealed that S61 is a PTM site (phosphoserine) based on the protein band migration pattern of S61R protein variant, which was lower compared to wild-type TMEM163 and other protein variants.

To provide additional confirmation that the decline of zinc efflux activity among non-synonymous SNPs and D124A/D128A constructs was not caused by diminished cell health, we performed cell viability assays and found no indication of cytotoxicity in these cells (**Fig. 5**). Although the cells expressing the S95C construct exhibited relatively lower viability, the values were not significant when compared to wild-type TMEM163 and other treatments. Overall, all the experimental results provide compelling evidence that TMEM163 is a zinc effluxer, and that non-synonymous SNP or mutation that potentially alters its structure results in abnormal transport activity. The diagram shown on Figure 5 summarizes the main findings of the study.

Mouse Tmem163 transcript expression is not exclusive to the brain

To address the previous report that the expression of mouse Tmem163 is only detected in the brain tissue (Burre *et al.*, 2007), we searched for publicly available RNA-seq data on Tmem163 expression. We found the Mouse ENCODE transcriptome data, which clearly identified the presence of *Tmem163* transcripts in several tissues, in addition to the cerebral cortex and cerebellum. Relatively high expression levels were seen in heart, lung, and spleen (**Supplemental Figure S6**), suggesting that Tmem163 may serve an important role in these tissues.

DISCUSSION

Our investigations on the function of TMEM163 using two different human cell lines and several independent techniques to evaluate the direction of zinc flux ultimately revealed that TMEM163 serves to transport zinc out of the cell or the cytoplasm. Our interests on human TMEM163 protein stemmed from our previous discovery that it is an interaction partner of the Transient Receptor Potential Mucolipin-1 (TRPML1) protein (Cuajungco *et al.*, 2014). Recently, it was shown that rodent Tmem163 interacts with itself and forms a functional dimer (Waberer *et al.*, 2017). Despite being predicted as an efflux transporter, earlier reports on rodent Tmem163 (Barth *et al.*, 2011; Waberer *et al.*, 2017) and our work on human TMEM163 (Cuajungco and Kiselyov, 2017) have suggested that the protein might be operating as an influx transporter. A case in point, it was reported that PC12 cells that heterologously express rodent Tmem163 displayed a noticeable rise in MP-FZ3 fluorescence within the cytoplasm upon exposure to zinc (Barth *et al.*, 2011). This report suggested that Tmem163 transports extracellular zinc inside the cells (Barth *et al.*, 2011). Furthermore, the same group showed that purified Tmem163 in liposomes mediate luminal zinc accumulation as evidenced by Fluozin-1 fluorescent dye when these lipid nanodiscs were exposed to exogenous zinc (Waberer *et al.*, 2017). In our previous preliminary study, TMEM163-expressing HEK-293 cells incubated with zinc produce a discernible up-regulation of MT-1A transcripts when compared with control cells after twenty-four hours (Cuajungco and Kiselyov, 2017), which suggests that TMEM163 could be an influxer. In contrast, when we knocked down TMEM163 expression in HEK-293 cells using RNAi, the fluorescence intensity of MP-FZ3 dye inside the cells remains considerably higher than control cells (Cuajungco *et al.*, 2014). After carefully re-analyzing these seemingly contradictory observations and performing additional experiments in the current study, we concluded that TMEM163 may actually be bringing zinc out of the cells in response to high cytosolic zinc levels. We believe that endogenous zinc transporters (e.g. ZNTs and ZIPs) confounded our previous interpretation of increased MT-1A transcript levels upon TMEM163 expression. It may be that over-expressing TMEM163 increased zinc extrusion from the cells, but that this effect induced a compensatory exogenous zinc uptake through native zinc influxers, which subsequently increased the expression of MT-

1A. In support of this supposition, transcripts of several zinc influx *SLC39* (*ZIP*) genes (e.g. ZIP1, ZIP3, ZIP6-ZIP10, ZIP13, and ZIP14) are detected in HEK-293 and HeLa cells (www.proteinatlas.org). Meanwhile, transcripts of some *SLC30* (*ZNT*) genes are also detected in HEK-293 cells (e.g. ZNT5 and ZNT6) and HeLa cells (e.g. ZNT1, ZNT5, and ZNT6) (www.proteinatlas.org). Indeed, Waberer and colleagues (2017) circumvented the potential confounding effects of native zinc influx and efflux proteins by using artificial liposomes. In their report, they purified rodent Tmem163 proteins and inserted them into lipid nanodiscs. This approach allowed them to show that Tmem163 binds to and transports zinc as evidenced by an increase in cell membrane permeant Fluozin-1 fluorescence inside the liposomes (Waberer *et al.*, 2017). While this elegant technique provided evidence for Tmem163-mediated zinc transport, it did not show whether the protein is an influxer or effluxer in living cells. Despite challenges in utilizing human cell lines, we successfully showed that TMEM163 extrudes zinc out of the cytoplasm upon intracellular zinc elevation. With regard to the Michaelis-Menten kinetics obtained for TMEM163 (Km = 8 μM), its transport activity emerges to be highly comparable to what others have reported for other zinc transporters such as ZIP1 (Km = 3 μM; (Gaither and Eide, 2001)), Zip5 (Km = 2 μM; (Wang *et al.*, 2004b)), and ZnT10 (Km = 2 μM; (Levy *et al.*, 2019)). The higher zinc transport kinetics previously reported for rodent Tmem163 (Km = 44 μM) (Waberer *et al.*, 2017) could be explained methodological difference, whereby we used radionuclide ^{65}Zn and human TMEM163 expressed in living cells, while the other group utilized a fluorescent dye and rodent Tmem163 present in a cell-free system. Notwithstanding, the kinetics of zinc efflux from our radionuclide ^{65}Zn assay is more physiologically relevant, particularly in the brain where TMEM163 is highly expressed (Cuajungco *et al.*, 2014) and where chelatable zinc released within neuronal synapse could reach up to micromolar levels (Howell *et al.*, 1984).

The dramatic negative response of TMEM163-D124A/D128A mutation on zinc efflux in comparison to ZIP1 and pmCherry vector control was unexpected, because if these mutations actually inactive the protein as has been reported for rodent Tmem163-D123A/D127A (Waberer *et al.*, 2017), then we would expect the fluorescence signal to be similar in magnitude to that of pmCherry empty vector control. Our data show that the depressed efflux activity of the double mutation is not due to mis-localization and/or cell toxicity as demonstrated by fluorescence imaging and viability assays, respectively. It is conceivable that the TMEM163-D124A/D128A monomer acts in a dominant negative manner upon dimerization with native TMEM163 monomers present in HEK-293 cells. We also cannot rule out the prospect that TMEM163-D124A/D128A may interact and induce a dominant negative effect on native zinc transporters present in cells (e.g. ZNTs), since various zinc efflux transporters have been reported to form heterodimers (Fukunaka *et al.*, 2009; Salazar *et al.*, 2009; Lasry *et al.*, 2014; Golan *et al.*, 2015). It would be interesting to find out in future studies if TMEM163-D124A/D128A's ability to dimerize with wild-type TMEM163 or potential to interact with other zinc transporters is the main reason for its dominant negative effect on efflux activity. Nevertheless, the negative effect of the double aspartate mutation on the role of TMEM163 is further substantiation that it is a zinc efflux transporter.

For experiments studying the consequence of non-synonymous SNPs in HEK-293 cells, we found that the amino acid substitution in three serine residues (S61R, S95C, and S193P) or in one glutamic acid residue (E286K) completely reduced TMEM163's zinc efflux activity. Interestingly, the CSB and WB results confirmed our *in silico* analysis that S61 is a PTM site, and that the arginine substitution in S61R variant disrupts protein modification based on the protein band migration pattern on the blot when compared with wild-type TMEM163 and other protein variants. It would be interesting in future studies to determine other PTM sites predicted to be located within the N-terminus of TMEM163, and to identify specific enzymes that are involved in the modification of this region. Meanwhile, the apparent mis-localization of S193P regardless of its C-terminus tag (mCherry fluorescent protein or dual Myc-DDK peptide), suggests that the proline substitution within the predicted TM4 of TMEM163 could have kinked this domain's alpha-helical structure (Grimm *et al.*, 2007; Cuajungco and Samie, 2008) such that it induced a conformational change. Interestingly, the mis-localization of S193P appears to be more severe in the presence of the mCherry fluorescent protein tag, possibly due to the size of mCherry, which has a molecular mass of 26.7 kDa (Shaner *et al.*, 2004). The reduction of PM localization also explains why the S193P protein variant has a lower efflux activity compared to the wild-type protein. On another note, it is not clear why the zinc efflux activity of E286K is dramatically reduced, which is virtually comparable to D124A/D128A variant. It is plausible that the change from a negatively charged glutamate to a positively charged lysine residue altered the protein's structure, which then created a dominant negative mutant like

that of the D124A/D128A protein variant. Future studies on TMEM163 structure and function could explain the probable dominant negative effect of site-specific mutations within the protein. Nevertheless, the reduction of zinc efflux activity observed from these non-synonymous SNPs provided additional support that TMEM163 is an effluxer.

Our investigations of the relationship between CDF family of proteins and TMEM163 indicate that TMEM163 should be classified as a unique CDF member that has a long N- and short C-terminus regions, since many CDF proteins such as the ZNT have short N- and long C-termini. Meanwhile, our analysis of the mouse Tmem163 transcript expression suggests that, like its human counterpart (Cuajungco *et al.*, 2014), this gene is convincingly detected in various tissues and is not exclusively expressed in the mouse brain as previously reported (Burre *et al.*, 2007). Whether the observed mouse transcripts in tissues other than the brain are translated into functional protein need further investigation and is beyond the scope of the current study.

In conclusion, our findings reveal that TMEM163 may play a crucial role in cellular zinc homeostasis by extruding cytoplasmic zinc ions outside of the cells. Future investigations on the importance of TMEM163 in select human tissues or organs, and its potential contributions to normal and pathological states are therefore warranted.

ACKNOWLEDGMENTS

We are very grateful to Theodros Kidane, Lauren Rosas, Cathleen Nguyen, Quinlan Cantrell, and Joshua Silva for their technical support. We also thank Dr. Sean Murray (CSU Northridge) for reading and critiquing the manuscript.

FUNDING SOURCE

MPC is funded by the National Institutes of Health (NIH) NINDS AREA grant R15 NS101594. VS was supported by the NIH NIGMS MARC U*STAR T34 GM008612 training grant. The content of this paper is solely the responsibility of the authors and does not necessarily represent the official views of the NIH.

CONFLICTS OF INTEREST

The authors declare no conflicts of interest with the contents of this article.

AUTHOR CONTRIBUTIONS

MPC conceived and designed the study, analyzed and interpreted data, wrote the manuscript, and project administration. VBS performed experiments, analyzed data, and edited the manuscript. SA performed experiments including assay optimization, analyzed data, and edited the manuscript. AE performed experiments and edited the manuscript. All authors read and approved the final version of the manuscript.

References

Ahn, Y.H., Kim, Y.H., Hong, S.H., Koh, J.Y. (1998) Depletion of intracellular zinc induces protein synthesis-dependent neuronal apoptosis in mouse cortical culture. Exp Neurol 154, 47-56.

Aiken, S.P., Horn, N.M., Saunders, N.R. (1992) Effects of histidine on tissue zinc distribution in rats. BioMetals 5, 235-243.

Aydemir, T.B., Kim, M.H., Kim, J., Colon-Perez, L.M., Banan, G., Mareci, T.H., Febo, M., Cousins, R.J. (2017) Metal Transporter Zip14 (Slc39a14) Deletion in Mice Increases Manganese Deposition and Produces Neurotoxic Signatures and Diminished Motor Activity. J Neurosci 37, 5996-6006.

Barth, J., Zimmermann, H., Volknandt, W. (2011) SV31 is a Zn2+-binding synaptic vesicle protein. J Neurochem 118, 558-570.

Beyer, N., Coulson, D.T., Heggarty, S., Ravid, R., Irvine, G.B., Hellemans, J., Johnston, J.A. (2009) ZnT3 mRNA levels are reduced in Alzheimer's disease post-mortem brain. Mol Neurodegener 4, 53.

Bosomworth, H.J., Adlard, P.A., Ford, D., Valentine, R.A. (2013) Altered expression of ZnT10 in Alzheimer's disease brain. PLoS One 8, e65475.

Burre, J., Zimmermann, H., Volknandt, W. (2007) Identification and characterization of SV31, a novel synaptic vesicle membrane protein and potential transporter. J Neurochem 103, 276-287.

Choi, B.Y., Kim, I.Y., Kim, J.H., Kho, A.R., Lee, S.H., Lee, B.E., Sohn, M., Koh, J.Y., Suh, S.W. (2016) Zinc transporter 3 (ZnT3) gene deletion reduces spinal cord white matter damage and motor deficits in a murine MOG-induced multiple sclerosis model. Neurobiol Dis 94, 205-212.

Choi, D.W., Yokoyama, M., Koh, J. (1988) Zinc neurotoxicity in cortical cell culture. Neuroscience 24, 67-79.

Colvin, R.A., Holmes, W.R., Fontaine, C.P., Maret, W. (2010) Cytosolic zinc buffering and muffling: their role in intracellular zinc homeostasis. Metallomics 2, 306-317.

Cuajungco, M.P., Basilio, L.C., Silva, J., Hart, T., Tringali, J., Chen, C.C., Biel, M., Grimm, C. (2014) Cellular zinc levels are modulated by TRPML1-TMEM163 interaction. Traffic 15, 1247-1265.

Cuajungco, M.P., Goldstein, L.E., Nunomura, A., Smith, M.A., Lim, J.T., Atwood, C.S., Huang, X., Farrag, Y.W., Perry, G., Bush, A.I. (2000) Evidence that the beta-amyloid plaques of Alzheimer's disease represent the redox-silencing and entombment of abeta by zinc. J Biol Chem 275, 19439-19442.

Cuajungco, M.P., Kiselyov, K. (2017) The mucolipin-1 (TRPML1) ion channel, transmembrane-163 (TMEM163) protein, and lysosomal zinc handling. Front Biosci (Landmark Ed) 22, 1330-1343.

Cuajungco, M.P., Lees, G.J. (1996) Prevention of zinc neurotoxicity in vivo by N,N,N',N'-tetrakis (2-pyridylmethyl) ethylene-diamine (TPEN). Neuroreport 7, 1301-1304.

Cuajungco, M.P., Lees, G.J. (1997a) Zinc and Alzheimer's disease: is there a direct link? Brain Res Brain Res Rev 23, 219-236.

Cuajungco, M.P., Lees, G.J. (1997b) Zinc metabolism in the brain: relevance to human neurodegenerative disorders. Neurobiol Dis 4, 137-169.

Cuajungco, M.P., Lees, G.J. (1998) Diverse effects of metal chelating agents on the neuronal cytotoxicity of zinc in the hippocampus. Brain Res 799, 97-107.

Cuajungco, M.P., Samie, M.A. (2008) The varitint-waddler mouse phenotypes and the TRPML3 ion channel mutation: cause and consequence. Pflugers Arch 457, 463-473.

Danscher, G., Jensen, K.B., Frederickson, C.J., Kemp, K., Andreasen, A., Juhl, S., Stoltenberg, M., Ravid, R. (1997) Increased amount of zinc in the hippocampus and amygdala of Alzheimer's diseased brains: a proton-induced X-ray emission spectroscopic analysis of cryostat sections from autopsy material. J Neurosci Methods 76, 53-59.

Eichelsdoerfer, J.L., Evans, J.A., Slaugenhaupt, S.A., Cuajungco, M.P. (2010) Zinc dyshomeostasis is linked with the loss of mucolipidosis IV-associated TRPML1 ion channel. J Biol Chem 285, 34304-34308.

Eide, D.J. (2006) Zinc transporters and the cellular trafficking of zinc. Biochim Biophys Acta 1763, 711-722.

Frederickson, C.J., Suh, S.W., Koh, J.Y., Cha, Y.K., Thompson, R.B., LaBuda, C.J., Balaji, R.V., Cuajungco, M.P. (2002) Depletion of intracellular zinc from neurons by use of an extracellular chelator in vivo and in vitro. J Histochem Cytochem 50, 1659-1662.

Fukunaka, A., Suzuki, T., Kurokawa, Y., Yamazaki, T., Fujiwara, N., Ishihara, K., Migaki, H., Okumura, K., Masuda, S., Yamaguchi-Iwai, Y., Nagao, M., Kambe, T. (2009) Demonstration and characterization of the heterodimerization of ZnT5 and ZnT6 in the early secretory pathway. J Biol Chem 284, 30798-30806.

Gaither, L.A., Eide, D.J. (2001) The human ZIP1 transporter mediates zinc uptake in human K562 erythroleukemia cells. J Biol Chem 276, 22258-22264.

Gee, K.R., Zhou, Z.L., Qian, W.J., Kennedy, R. (2002) Detection and imaging of zinc secretion from pancreatic beta-cells using a new fluorescent zinc indicator. J Am Chem Soc 124, 776-778.

Golan, Y., Berman, B., Assaraf, Y.G. (2015) Heterodimerization, altered subcellular localization, and function of multiple zinc transporters in viable cells using bimolecular fluorescence complementation. J Biol Chem 290, 9050-9063.

Grimm, C., Cuajungco, M.P., van Aken, A.F., Schnee, M., Jors, S., Kros, C.J., Ricci, A.J., Heller, S. (2007) A helix-breaking mutation in TRPML3 leads to constitutive activity underlying deafness in the varitint-waddler mouse. Proc Natl Acad Sci U S A 104, 19583-19588.

Hofmann, K., Stoffel, W. (1993) TMbase - A database of membrane spanning proteins segments. Biol Chem 374, 166.

Horn, N.M., Thomas, A.L., Tompkins, J.D. (1995) The effect of histidine and cysteine on zinc influx into rat and human erythrocytes. J Physiol 489 (Pt 1), 73-80.

Howell, G.A., Welch, M.G., Frederickson, C.J. (1984) Stimulation-induced uptake and release of zinc in hippocampal slices. Nature 308, 736-738.

Itoh, M., Ebadi, M., Swanson, S. (1983) The presence of zinc-binding proteins in brain. J Neurochem 41, 823-829.

Kambe, T., Hashimoto, A., Fujimoto, S. (2014) Current understanding of ZIP and ZnT zinc transporters in human health and diseases. Cell Mol Life Sci 71, 3281-3295.

Kaneko, M., Noguchi, T., Ikegami, S., Sakurai, T., Kakita, A., Toyoshima, Y., Kambe, T., Yamada, M., Inden, M., Hara, H., Oyanagi, K., Inuzuka, T., Takahashi, H., Hozumi, I. (2015) Zinc transporters ZnT3 and ZnT6 are downregulated in the spinal cords of patients with sporadic amyotrophic lateral sclerosis. J Neurosci Res 93, 370-379.

Kim, J., Kim, T.Y., Hwang, J.J., Lee, J.Y., Shin, J.H., Gwag, B.J., Koh, J.Y. (2009) Accumulation of labile zinc in neurons and astrocytes in the spinal cords of G93A SOD-1 transgenic mice. Neurobiol Dis 34, 221-229.

Koh, J.Y., Choi, D.W. (1994) Zinc toxicity on cultured cortical neurons: involvement of N-methyl-D-aspartate receptors. Neuroscience 60, 1049-1057.

Koh, J.Y., Suh, S.W., Gwag, B.J., He, Y.Y., Hsu, C.Y., Choi, D.W. (1996) The role of zinc in selective neuronal death after transient global cerebral ischemia. Science 272, 1013-1016.

Kukic, I., Kelleher, S.L., Kiselyov, K. (2014) Zinc efflux through lysosomal exocytosis prevents zinc-induced toxicity. J Cell Sci 127, 3094-3103.

Lasry, I., Golan, Y., Berman, B., Amram, N., Glaser, F., Assaraf, Y.G. (2014) In situ dimerization of multiple wild type and mutant zinc transporters in live cells using bimolecular fluorescence complementation. J Biol Chem 289, 7275-7292.

Levy, M., Elkoshi, N., Barber-Zucker, S., Hoch, E., Zarivach, R., Hershfinkel, M., Sekler, I. (2019) Zinc transporter 10 (ZnT10)-dependent extrusion of cellular Mn(2+) is driven by an active Ca(2+)-coupled exchange. J Biol Chem 294, 5879-5889.

Medvedeva, Y.V., Lin, B., Shuttleworth, C.W., Weiss, J.H. (2009) Intracellular Zn2+ accumulation contributes to synaptic failure, mitochondrial depolarization, and cell death in an acute slice oxygen-glucose deprivation model of ischemia. J Neurosci 29, 1105-1114.

Ohana, E., Hoch, E., Keasar, C., Kambe, T., Yifrach, O., Hershfinkel, M., Sekler, I. (2009) Identification of the Zn2+ binding site and mode of operation of a mammalian Zn2+ transporter. J Biol Chem 284, 17677-17686.

Salazar, G., Falcon-Perez, J.M., Harrison, R., Faundez, V. (2009) SLC30A3 (ZnT3) oligomerization by dityrosine bonds regulates its subcellular localization and metal transport capacity. PLoS One 4, e5896.

Scarr, E., Udawela, M., Greenough, M.A., Neo, J., Suk Seo, M., Money, T.T., Upadhyay, A., Bush, A.I., Everall, I.P., Thomas, E.A., Dean, B. (2016) Increased cortical expression of the zinc transporter SLC39A12 suggests a breakdown in zinc cellular homeostasis as part of the pathophysiology of schizophrenia. NPJ Schizophr 2, 16002.

Shaner, N.C., Campbell, R.E., Steinbach, P.A., Giepmans, B.N., Palmer, A.E., Tsien, R.Y. (2004) Improved

monomeric red, orange and yellow fluorescent proteins derived from Discosoma sp. red fluorescent protein. Nat Biotechnol 22, 1567-1572.

Smailhodzic, D., van Asten, F., Blom, A.M., Mohlin, F.C., den Hollander, A.I., van de Ven, J.P., van Huet, R.A., Groenewoud, J.M., Tian, Y., Berendschot, T.T., Lechanteur, Y.T., Fauser, S., de Bruijn, C., Daha, M.R., van der Wilt, G.J., Hoyng, C.B., Klevering, B.J. (2014) Zinc supplementation inhibits complement activation in age-related macular degeneration. PLoS One 9, e112682.

Spyropoulos, I.C., Liakopoulos, T.D., Bagos, P.G., Hamodrakas, S.J. (2004) TMRPres2D: high quality visual representation of transmembrane protein models. Bioinformatics 20, 3258-3260.

Waberer, L., Henrich, E., Peetz, O., Morgner, N., Dotsch, V., Bernhard, F., Volknandt, W. (2017) The synaptic vesicle protein SV31 assembles into a dimer and transports Zn(2). J Neurochem 140, 280-293.

Wang, F., Dufner-Beattie, J., Kim, B.E., Petris, M.J., Andrews, G., Eide, D.J. (2004a) Zinc-stimulated endocytosis controls activity of the mouse ZIP1 and ZIP3 zinc uptake transporters. J Biol Chem 279, 24631-24639.

Wang, F., Kim, B.E., Petris, M.J., Eide, D.J. (2004b) The mammalian Zip5 protein is a zinc transporter that localizes to the basolateral surface of polarized cells. J Biol Chem 279, 51433-51441.

Yoo, M.H., Lee, J.Y., Lee, S.E., Koh, J.Y., Yoon, Y.H. (2004) Protection by pyruvate of rat retinal cells against zinc toxicity in vitro, and pressure-induced ischemia in vivo. Invest Ophthalmol Vis Sci 45, 1523-1530.

Zalewski, P.D., Forbes, I.J., Betts, W.H. (1993) Correlation of apoptosis with change in intracellular labile Zn(II) using zinquin [(2-methyl-8-p-toluenesulphonamido-6-quinolyloxy)acetic acid], a new specific fluorescent probe for Zn(II). Biochem J 296 (Pt 2), 403-408.

Zhao, J., Bertoglio, B.A., Gee, K.R., Kay, A.R. (2008) The zinc indicator FluoZin-3 is not perturbed significantly by physiological levels of calcium or magnesium. Cell Calcium 44, 422-426.

FIGURE LEGENDS

Figure 1. Functional expression of TMEM163 stably expressed in HeLa cells. A) Cell membrane impermeant Fluozin-3 (MI-FZ3) fluorescence analysis revealed a significant increase in extracellular RFU levels in the milieu of cells expressing TMEM163-mCherry upon exposure to zinc. Data are represented as mean ± SEM (*****p* < 0.0001, Student's *t*-test, unpaired, two-tailed; n = 5 independent trials). **B**) Cell membrane permeant Newport Green (MP-NG) fluorescence analysis revealed a significant decrease in intracellular RFU levels of cells expressing TMEM163-mCherry upon exposure to zinc when compared with cells expressing the pmCherry vector control. Data are represented as mean ± SEM of each kinetic time point analyzed (**p* = 0.01; Student's *t*-test, unpaired, two-tailed; n = 6 independent trials). **C**) Concentration dependence and saturable uptake of ^{65}Zn by TMEM163-expressing cells with apparent Michaelis-Menten (Km) value of 8 μM and Vmax of 98 pmol/min/mg total protein (*p* = 0.01; Student's *t*-test, paired, two-tailed; n = 3 independent trials).

Figure 2. Spectrofluorometric assay and fluorescence microscopy of HEK-293 cells transiently expressing wild-type TMEM163, TMEM163-D124A/128A, ZIP1, and pmCherry empty vector control. A) Cell membrane impermeant Fluozin-3 fluorescence analysis reveals a significant increase in extracellular fluorescence upon expression of TMEM163 protein when compared with controls. Data are represented as mean ± SEM of each kinetic time point analyzed (***p* = 0.002, *****p* < 0.0001; Tukey's multiple comparisons *post-hoc* test; n ≥ 5 independent trials). **B**) Representative fluorescent micrographs showing subcellular distribution of pmCherry (mCh) empty vector, TMEM163-mCherry, ZIP1-mCherry, and TMEM163-D124A/D128A-mCherry. TMEM163 and TMEM163-D124A/D128A localize within the plasma membrane and membrane compartments (*arrowhead*). ZIP1 is also detected within the plasma membrane and intracellular membrane compartment (*arrowhead*). The pmCherry vector exclusively localizes in the cytoplasm (*arrow*). Scale bar: 50 μm.

Figure 3. Spectrofluorometric assay and fluorescence microscopy of HEK-293 cells transiently expressing wild-type TMEM163 and non-synonymous SNPs: S61R, S95C, S193P, and E286K. A) Cell membrane impermeant Fluozin-3 fluorescence analysis reveals a significant increase in extracellular fluorescence upon expression of TMEM163 protein. Non-synonymous SNPs negatively affect the efflux function of TMEM163, particularly the E286K clone. Data are represented as mean ± SEM of each kinetic time point analyzed (**p* = 0.04, ***p* = 0.004, ****p* = 0.0004; Tukey's multiple comparisons *post-hoc* test; n ≥ 4 independent trials). **B**) Representative fluorescent micrographs of expression constructs with mCherry (mCh) fluorescent protein tag (*top panel*) and Myc-DDK peptide tag probed with Alexa Fluor-488 (A488) (*bottom panel*). TMEM163-S61R, TMEM163-S95C, and TMEM163-E286K exhibit localization within the plasma membrane and intracellular membrane compartment (*arrowhead*), while TMEM163-S193P shows mostly cytoplasmic and compartmental localization (*arrow*). Scale bar: 50 μm.

Figure 4. Cell surface expression of wild-type TMEM163, TMEM163-D124A/D128A variant, and non-synonymous SNPs: S61R, S95C, S193P, and E286K. Representative Western blot images of Myc-DDK peptide tag constructs probed with anti-DDK monoclonal antibody following CSB (*left panel*) and standard immunoblot of cell lysates taken from each expression construct (*right panel*). All TMEM163 expression constructs show protein localization within the PM. The levels of PM localization for TMEM163-S193P (*green asterisk*) is noticeably reduced compared to the others variants, which supported fluorescence microscopy data. The blots also show that TMEM163-S61R (*purple arrowhead*) migrated faster than the wild-type TMEM163 and other protein variants due to the presence of arginine, which resulted in loss of post-translational modification. I, input; E, elution; (n = 3 independent trials).

Figure 5. Cell viability of HEK-293 cells expressing wild-type TMEM163, TMEM163-D124A/D128A variant, and non-synonymous SNPs: S61R, S95C, S193P, and E286K. The mammalian expression construct contains the mCherry fluorescent protein tag. The TMEM163 protein variants do not significantly affect cell survival when compared to cells expressing the wild-type TMEM163 construct. Note, however, that cells expressing the S95C construct appear to have slight cytotoxicity in comparison with the other expression constructs. Data are represented as mean ± SEM of % control (n ≥ 4 independent trials).

Figure 6. Schematic diagram summarizing the main observations on the zinc efflux function of TMEM163. Heterologous expression of the wild-type TMEM163 results in cytoplasmic zinc extrusion in the presence of high zinc levels inside the cells. Expression of the non-synonymous SNPs S61R, S95C, and S193P produces marked reduction of efflux activity when compared with wild-type TMEM163. S61R showed altered protein band migration pattern on WB, suggesting that S61 is a PTM target. S193P is mostly expressed in the cytoplasm and MC as evidenced by CSB and WB, while the other variants are found mostly in the PM and MC. The E286K protein variant has the lowest efflux activity in comparison with other SNPs and wild-type TMEM163. Similar to E283K, the D124A/D128A protein variant has comparably the lowest efflux activity relative to the wild-type TMEM163 and other SNPs. PM, plasma membrane; MC, membrane compartment.

Fig. 1

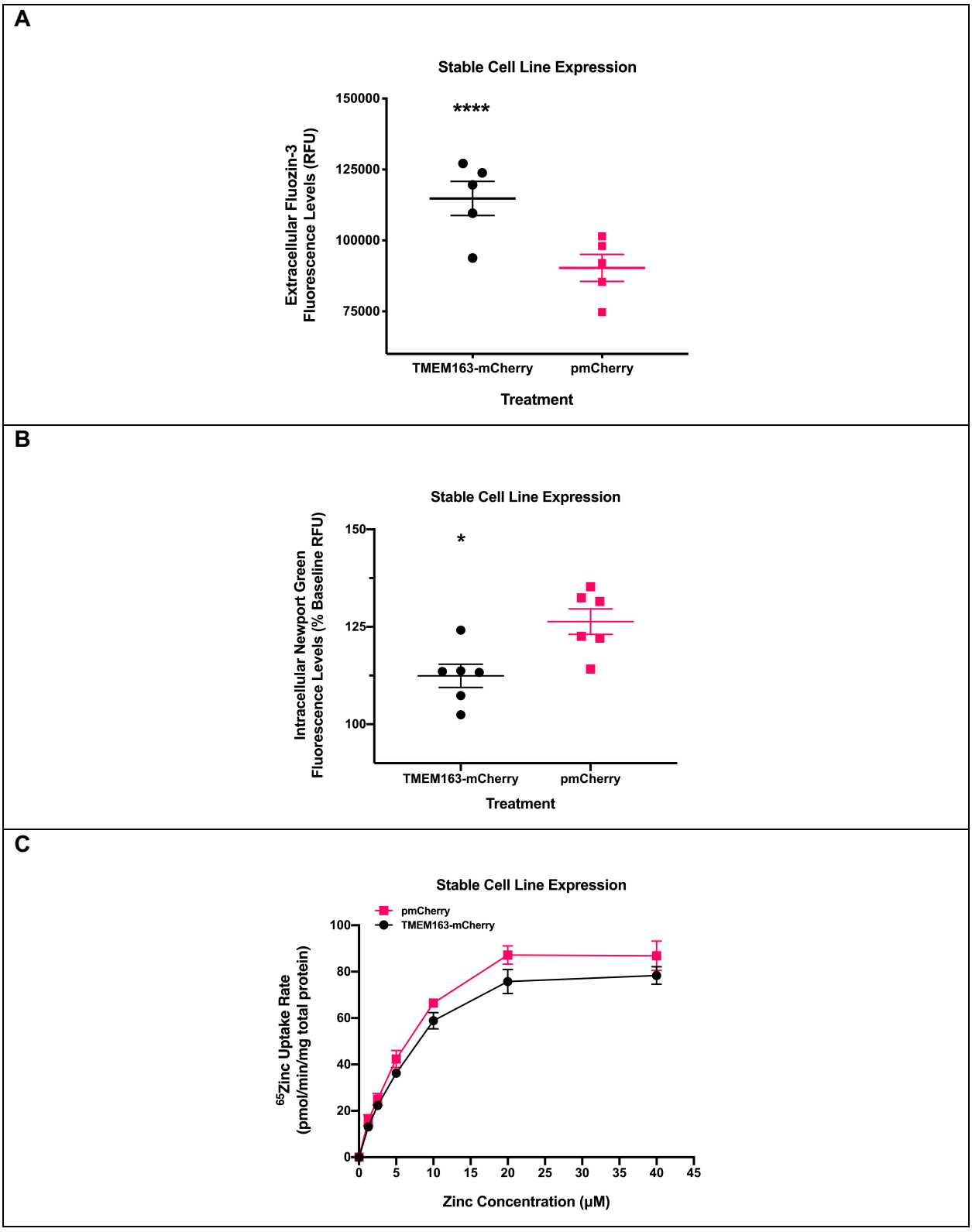

Fig. 2

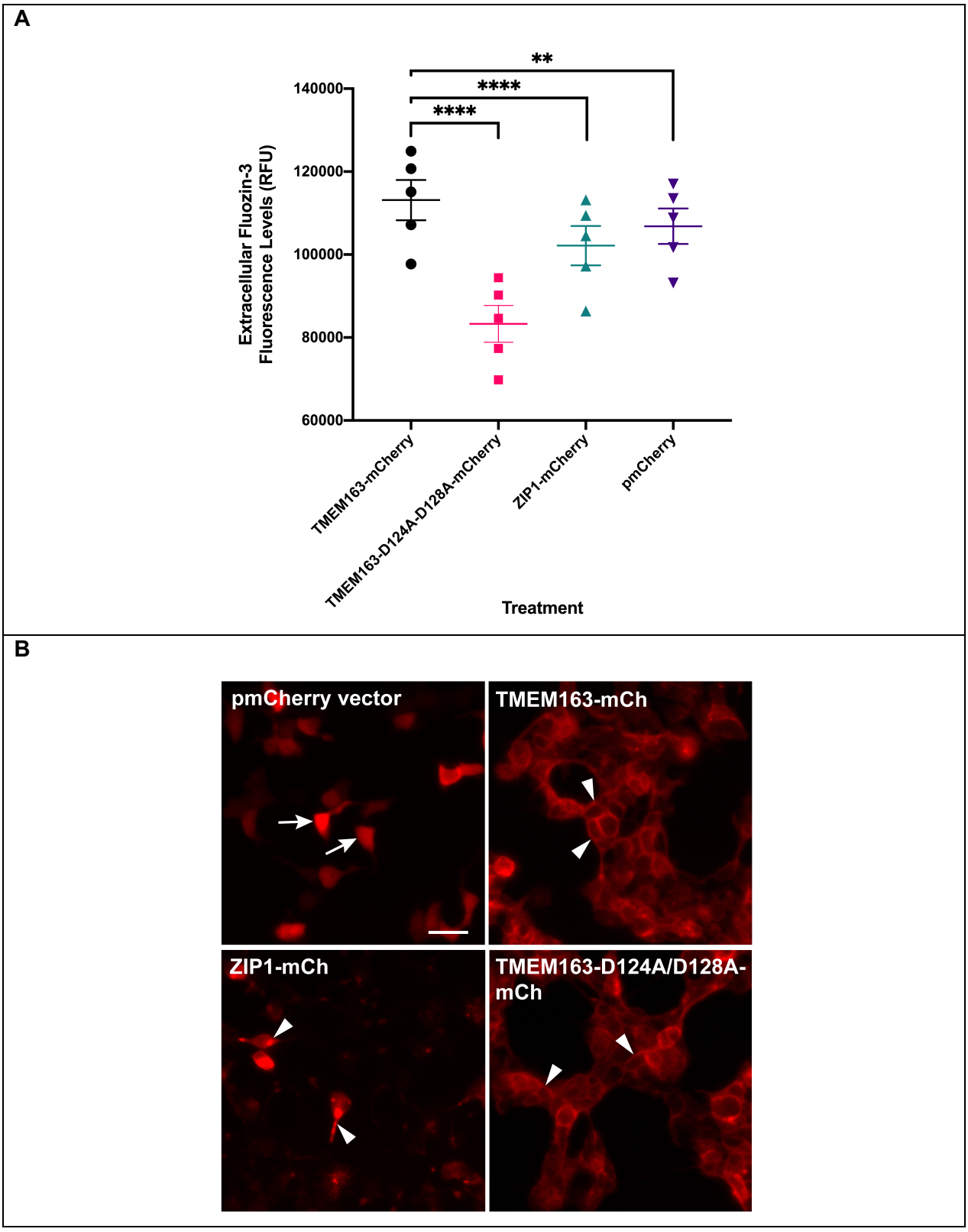

Fig. 3

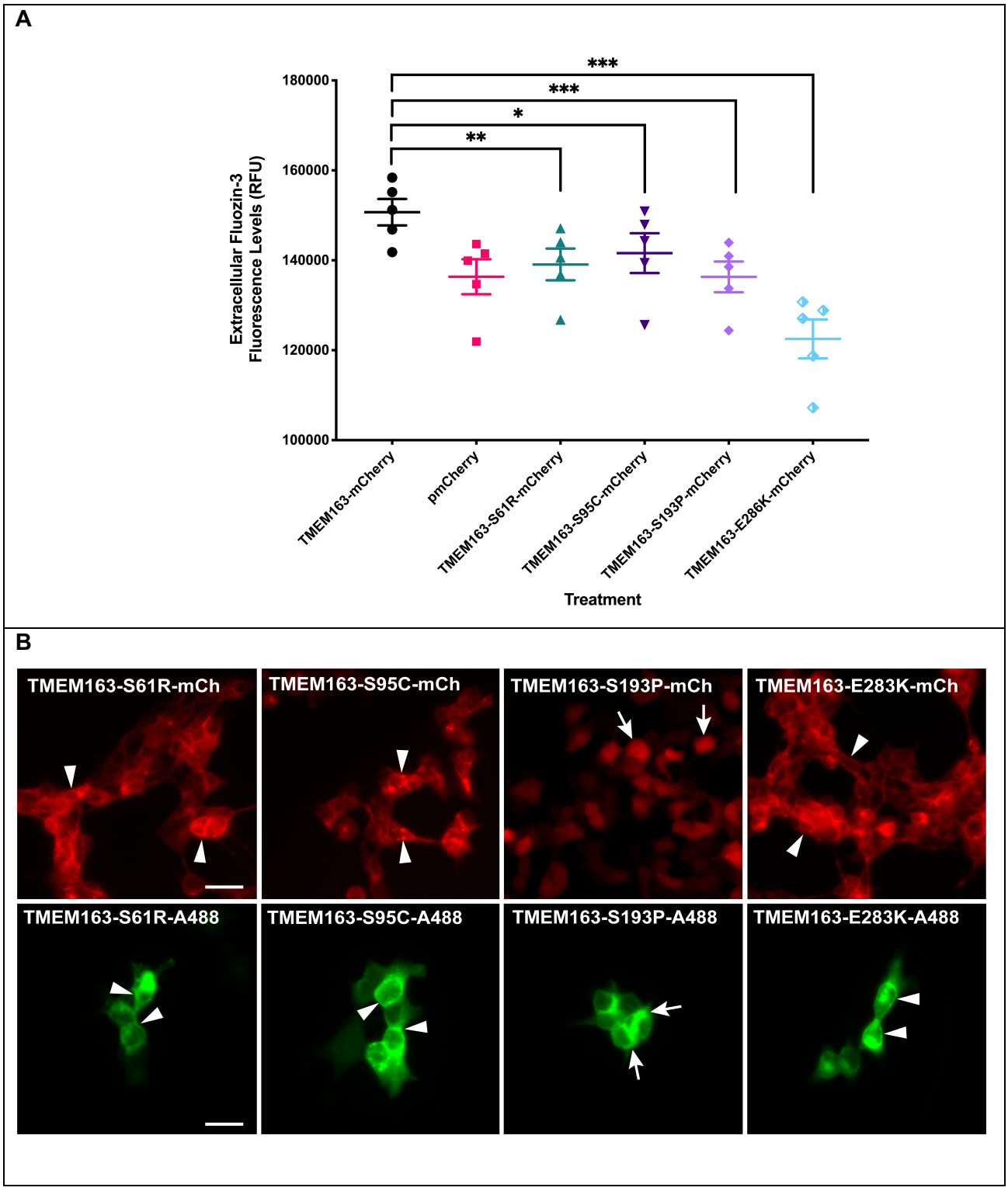

Fig. 4

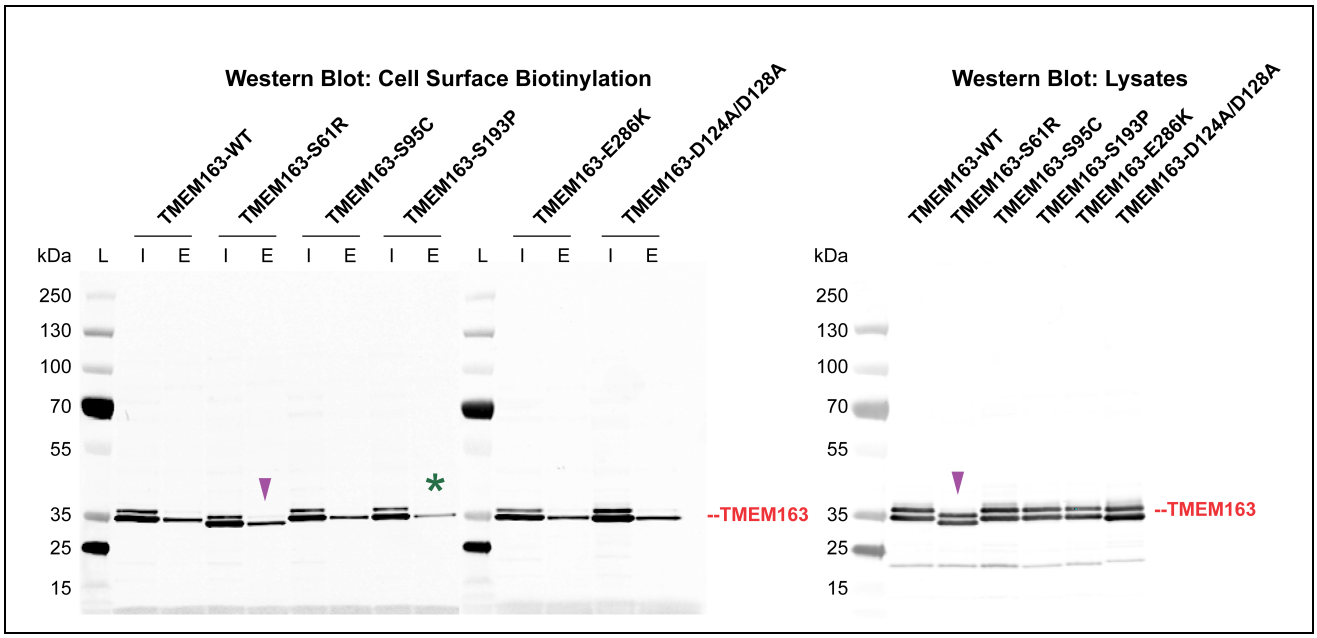

Fig. 5

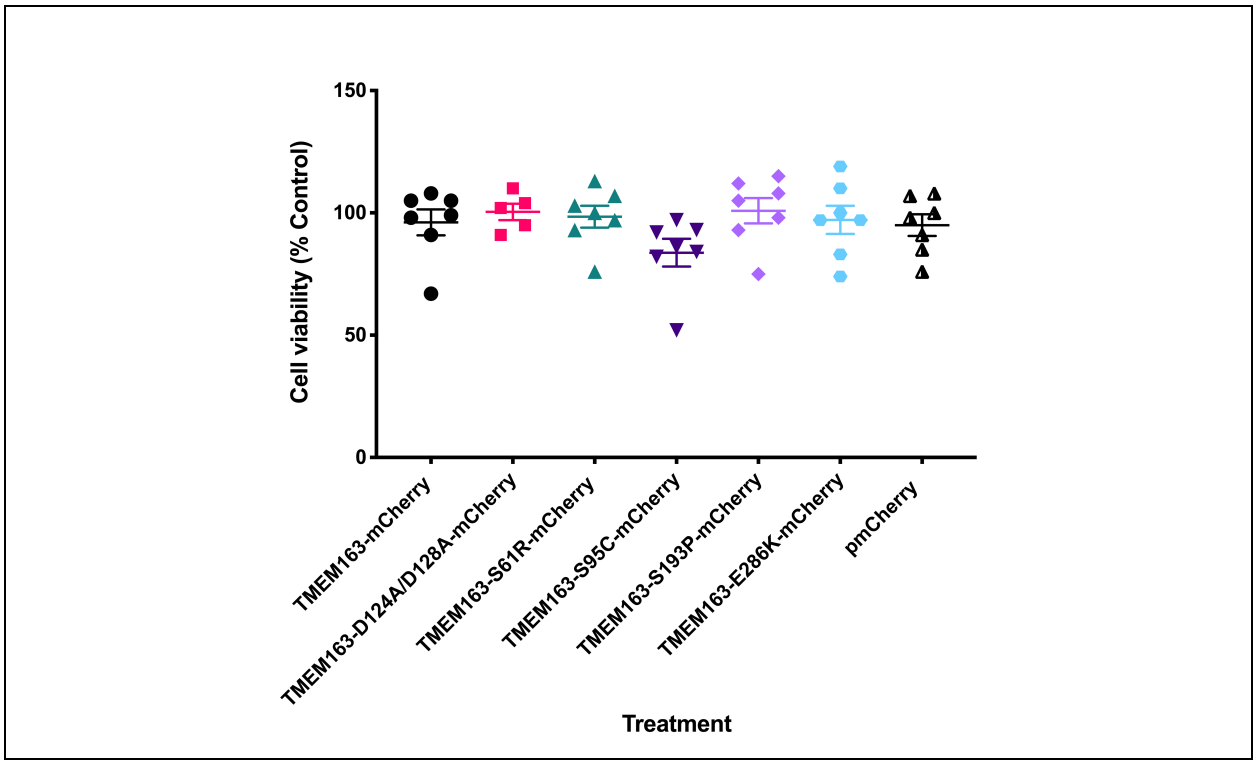

Fig. 6